Cite this article
Wen L, Li Y and Chai J
Plastic-damage analysis of concrete cutoff wall for a concrete face rockfill dam.
Proceedings of the Institution of Civil Engineers – Geotechnical Engineering,
https://doi.org/10.1680/jgeen.19.00006

Research Article
Paper 1900006
Received 07/01/2019;
Accepted 09/07/2019

Keywords: dams, barrages & reservoirs/diaphragm & in situ walls/stress analysis

Geotechnical Engineering

ice Publishing

Plastic-damage analysis of concrete cutoff wall for a concrete face rockfill dam

Lifeng Wen PhD
Lecturer, State Key Laboratory of Eco-hydraulics in Northwest Arid Region of China, Xi'an University of Technology, Xi'an, PR China

Junrui Chai PhD
Professor, State Key Laboratory of Eco-hydraulics in Northwest Arid Region of China, Xi'an University of Technology, Xi'an, PR China

Yanlong Li PhD
Professor, State Key Laboratory of Eco-hydraulics in Northwest Arid Region of China, Xi'an University of Technology, Xi'an, PR China
(corresponding author: lylong2356@126.com)

Through in situ measurement records and numerical analysis, this work investigated the behaviour of a concrete cutoff wall for a concrete face rockfill dam built on an alluvium foundation. Monitoring records were obtained from a detailed monitoring system. A three-dimensional numerical model that uses a plastic-damage model for the stress–strain relationship of concrete was developed to predict the behaviour of the concrete cutoff wall. A coupled hydro-mechanical (HM) method was adopted to characterise the HM coupling effect of the dam and the alluvium foundation. The dam construction and the subsequent reservoir-filling processes were simulated in the numerical model. The results were compared with in situ measurements to validate the numerical model. The loading mechanism, stress and deformation behaviour, damage distribution and cracking of the cutoff wall were analysed. The wall behaviour, especially with relevance to the walls for dams with corewalls or inclined corewalls, and the effects of several factors on wall behaviour were investigated.

Notation

C_c	curvature coefficient
C_u	non-uniformity coefficient
$\boldsymbol{D}$	tangential elastic modulus tensor
d	scalar degradation damage variable
d_T, d_C	tension and compressive uniaxial damage variables
E_0	deformation modulus
E_i	undamaged elastic stiffness
$\boldsymbol{f}_b$	body force tensor
G_0, F_0 D_0	model parameters
G_n	fracture energy
g_n	dissipated energy density of concrete
$H(\phi–z)$	Heaviside function
K	modulus number
K_n	normal contact stiffness
k, k_0	current and initial hydraulic conductivity
k_n	damage variable
k_T, k_C	tension and compressive damage variables
l_n	characteristic length
m	pressure index
N	blow number of standard penetration test
n_i, n_0	current and initial porosity
P	normal contact pressure
p_w	pore water pressure
R_f	failure ratio
S_w	specific storage
s	weight factor
t	time
$\boldsymbol{u}$	displacement vector
$\boldsymbol{v}$	flow velocity
α	Biot's coefficient
β_1	calculation coefficient
$\Delta\phi$	reductional friction angle
$\boldsymbol{\delta}$	Kronecker delta tensor
ε_0	invasion tolerance
ε	total strain
ε^p	plastic strain
ε_v	volume strain
λ_i, λ_{i+1}	Lagrange multiplier of iteration step i and $i+1$
μ_n	distance between two contact faces
ρ_w	water density
σ, σ_n, $\bar{\sigma}$	stress, uniaxial stress and effective stress
ϕ	total water head
ϕ_0	initial friction angle

1. Introduction

With an increase in energy demands and the evolution of construction methods, an increasing number of earth and rockfill dams have been, and are being, founded on pervious and highly compressible alluvial deposits. Cutoff walls are the most extensively used anti-seepage treatments in alluvium foundations. Such walls are less prone to deterioration than other methods and can provide a continuous seepage barrier (Bruce *et al.*, 2012; Moharrami *et al.*, 2014; Rosen *et al.*, 2011). During dam construction and reservoir filling, the foundation and wall are compressed under the weight of the dam embankment and water load. Consequently, the wall may undergo significant plastic straining, which can potentially lead to cracking. Case studies on long-term wall performance have encountered direct evidence of cutoff wall cracking (Rice and Duncan, 2010a). Even cracks with apertures less than 1·0 mm can increase the effective hydraulic conductivity of a seepage barrier by several orders of magnitude (Rice and Duncan, 2010b). Understanding wall behaviour is thus critical in designing optimisations and performance assessments.

The loading condition of a cutoff wall is complicated. The wall not only bears the weight of the dam and the water pressure caused by reservoir filling but it also has a complex interaction with the adjacent soil. Many laboratory tests have been performed to characterise the performance of cutoff wall materials (Abbaslou *et al*., 2016; Ata *et al*., 2015; Chegenizadeh *et al*., 2018; Hinchberger *et al*., 2010), but wall behaviour has rarely been tested directly (Xiao *et al*., 2016). Dascal (1979) and Takai *et al*. (2016) analysed the technical characteristics and structural performance of the cutoff walls of some dams, but vast differences were observed between different projects. Thus, limited insights into wall behaviour were obtained. Rice and Duncan (2010a) investigated the failure or cracking mechanisms of seepage barriers based on observations and insights from 30 case histories of earthen dams; they obtained significant insights into the long-term performance of such barriers, but focused only on seepage barriers used to repair existing dams.

Several investigators have performed numerical analyses on the behaviour of cutoff walls (Li *et al*., 2015; Yu *et al*., 2015), but the numerical results were unconfirmed with measured results and these studies did not involve in-depth analysis. The linear elastic model is extensively used for concrete cutoff walls. However, concrete exhibits linear elastic behaviour only under small loads. Cracking and damage will occur with an increase in tensile strain (Xu *et al*., 2015). Moreover, in previous studies (Wen *et al*., 2015; Xu *et al*., 2012; Yu *et al*., 2015), water pressure has constantly been simulated as a surface force and has been applied to impervious systems, with the seepage effect disregarded. The behaviour of rockfill dams depends on the mechanical and hydraulic properties of dam construction materials. The hydro-mechanical (HM) coupling (i.e. seepage field and stress field coupling) process can significantly affect dam behaviour, especially those built on an alluvium foundation that is below the free surface after reservoir filling. In addition, previous studies on the behaviour of concrete cutoff walls have involved dams with corewalls or inclined corewalls, with the cutoff wall located in the middle of the dam base. However, only a few studies (Wen *et al*., 2015, 2018) have been conducted on the behaviour of cutoff walls for concrete face rockfill dams (CFRDs) with the cutoff wall at the upstream face of the dam, despite the construction of a large number of this type of cutoff wall.

This paper describes a study based on in situ measurement records and numerical analysis of the behaviour of a cutoff wall for a CFRD. A three-dimensional (3D) numerical model that uses a plastic-damage model for the stress–strain relationship of concrete for predicting the behaviour of a concrete cutoff wall was developed. The soil–structure interface behaviour and the HM coupling effect were considered in the model. To verify the model, the numerical results were compared with in situ measurements. The loading mechanism, deformation behaviour, damage distribution and cracking of the wall were analysed and the effects of wall material and the HM coupling effect were also investigated.

2. Case study

2.1 Project information

The Miaojiaba project, consisting of a CFRD, a downstream power station and a diversion tunnel, is located in Bailongjiang River, Wenxian city, Gansu province, China. The dam height is 111 m, with a crest of 348·20 m in length and a normal water level of 800 m. The upstream dam slope is 1 : 1·4, whereas the downstream integrated slope is 1 : 1·55. Figure 1 shows the rockfill material zoning of the dam. The construction parameters and methods for the main rockfill and sub-rockfill zones were the same. Figure 1(a) shows details of the construction materials, compaction methods and construction process.

2.2 Site conditions

The dam site has 44–50 m thick deep alluvium along the V-shaped river valley over the bedrock. A series of in situ and laboratory tests was performed to obtain the physical and mechanical properties of the alluvium. Three layers were identified from top to bottom. The site comprises cobble, sand and gravel, with a gravel layer (Q_4^{a3}) of 6–20 m thickness underlain by a sand and gravel layer (Q_4^{a2}) of 12–15 m thickness that overlies a block and gravel layer (Q_4^{a1}) of 6–20 m thickness. Layer Q_4^{a2} is the main component of the alluvium. Beneath Q_4^{a1} is the metamorphic tuff bedrock. No large-scale faults or strong weathering zones have been observed in the bedrock.

Figure 2 shows the physical and mechanical properties of the alluvium obtained from a series of field and laboratory tests. The standard penetration test (SPT) N values were obtained using a standard 63·5 kg hammer free falling from a height of 76 cm. When the cumulative distance of driving was 10 cm, the total number of blows of the hammer was denoted by the blow count N. Given that the SPT was conducted only for the alluvium within the range of 35 m, no test data were obtained below a depth of 35 m. ϕ_0 is the internal angle of friction obtained from consolidated-undrained triaxial compression tests. E_0 is the deformation modulus, which was estimated from a pressure–volume relationship curve on an empirical basis through pressuremeter tests (Wang *et al*., 2008). k is the hydraulic conductivity. Horizontal and vertical hydraulic conductivities were measured through an in situ permeability test. As shown in Figure 2, the porosity was found to decrease with an increase in depth, accompanied by an increase in dry density. Alluvium commonly has a large porosity, a high shear strength and deformation modulus. The distribution of hydraulic conductivity (k) in the horizontal direction was similar to that in the vertical direction, but with larger values.

The particle size distribution of the alluvium is shown in Figure 3. The grain size covered an extensive range, with a maximum size of approximately 600 mm. For layers Q_4^{a1},

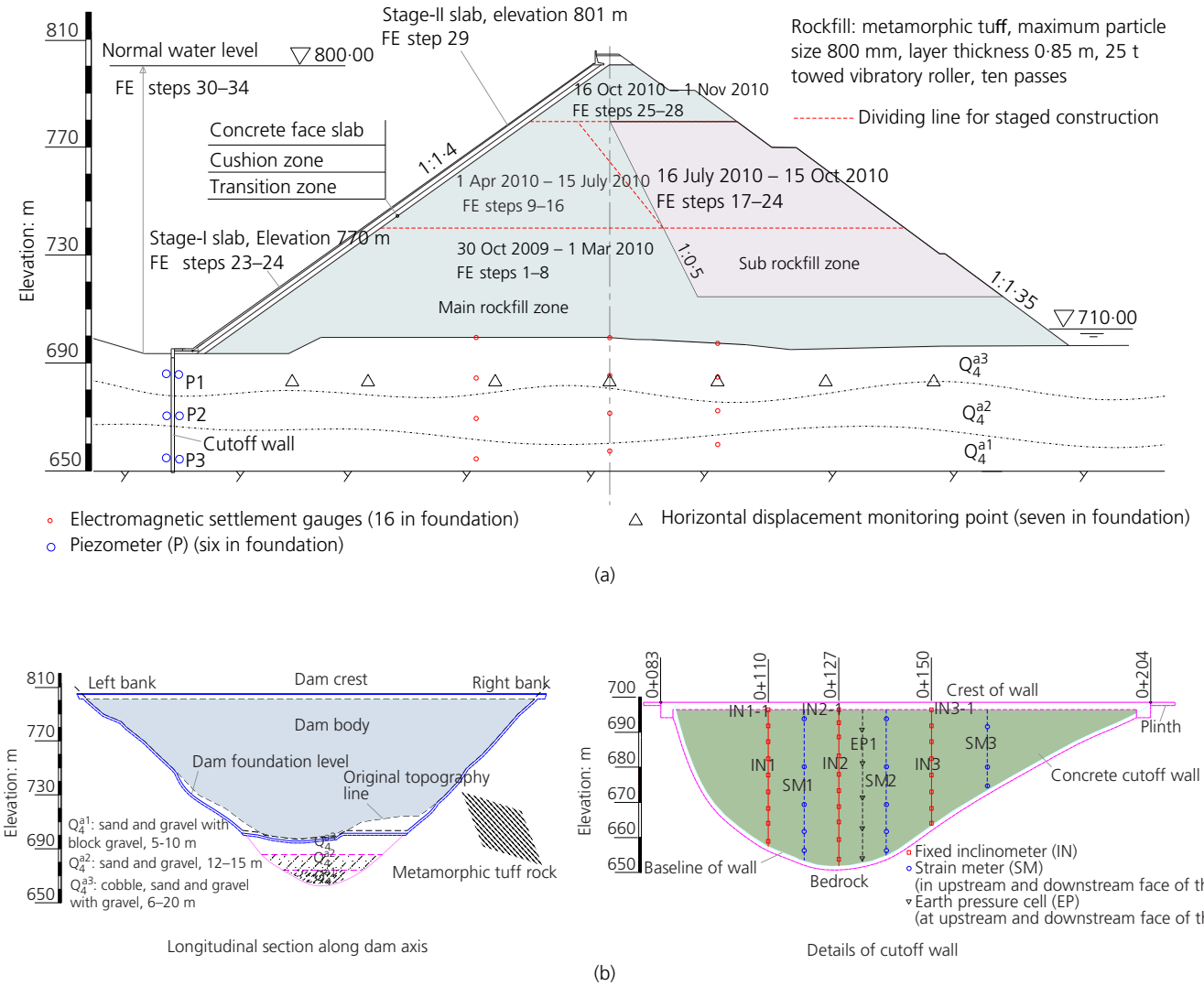

Figure 1. (a) Typical cross-section of Miaojiaba dam. (b) Longitudinal section along the dam axis and details of the cutoff wall

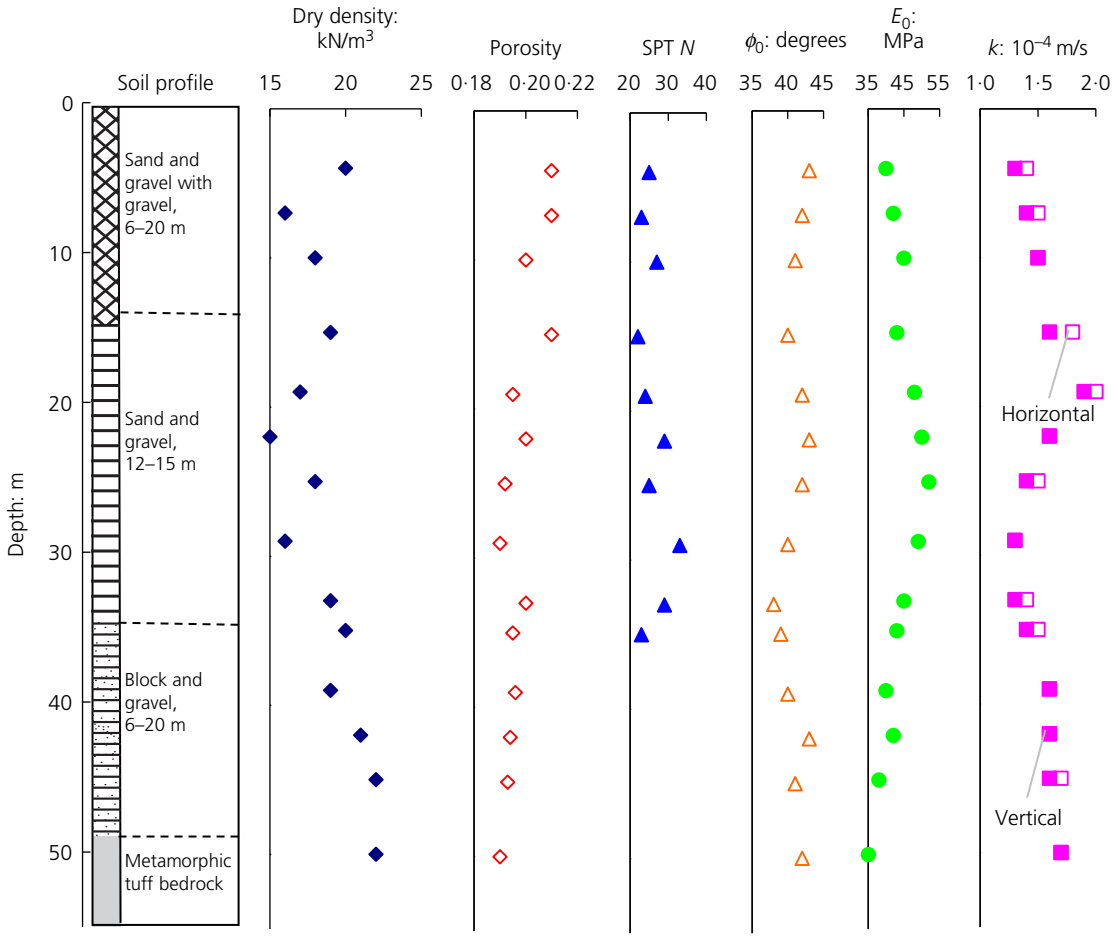

Figure 2. Physical and mechanical properties of the alluvium foundation

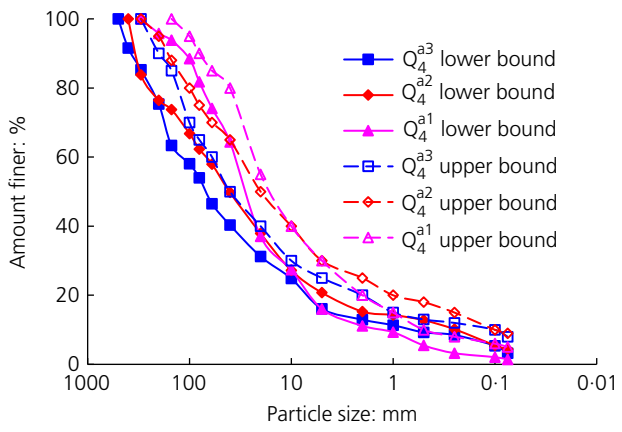

Figure 3. Gradation of the alluvium foundation

Q_4^{a2} and Q_4^{a3}, the coefficients of non-uniformity (C_u) of the lower range were determined to be 283, 200 and 237, while the coefficients of curvature (C_c) were 13·6, 4·3 and 10·6, respectively. These results imply that all layers of the alluvium are poorly graded. The alluvium is characterised by a loose structure, a wide particle size distribution, high permeability and inhomogeneity. The looseness and settlement of the surface layer were reduced by ten passes of compaction with a 2·2 m towed vibrating roller with a mass of 25 000 kg.

2.3 Design of the cutoff wall and monitoring instruments

A slot-type concrete cutoff wall was constructed in the alluvium foundation to control seepage flow in the foundation. The wall is 121 m long with a total area of 2900 m^2. The maximum depth is 50·5 m with a minimum penetration depth of approximately 0·5 m into the bedrock. The wall thickness is 1·2 m. Figure 1(b) shows a longitudinal section along the dam axis and details of the cutoff wall. The wall is composed of C30 concrete with standard values of axial compressive strength (20·1 MPa) and axial tensile strength (2·01 MPa) (Wang *et al.*, 2008). A panel-by-panel construction technique with a stop-end method (Arnold *et al.*, 2011; Song and Cui, 2015; Soroush and Soroush, 2005) was used. Construction of the wall began 3 months before construction of the dam.

Table 1. Details of the monitoring instruments installed in the foundation and cutoff wall

Instrumentation	Object of measurement	Description
Electromagnetic settlement gauges	Alluvium settlement	Three monitoring lines in section 0 + 194, shown in Figure 1(b)
Displacement transducers	Horizontal displacement	Seven monitoring points in section 0 + 194, shown in Figure 1(b)
Piezometers	Pore water pressure	Six monitoring points in alluvium foundation, shown in Figure 1(b)
Fixed inclinometers	Cutoff wall movement	Three groups in the wall, shown in Figure 1(a)
Strain meters	Vertical stress of cutoff wall	26 monitoring points symmetrically in the upstream face and downstream face of the wall, shown in Figure 1(b)
Earth pressure cells	Lateral earth pressure on cutoff wall	Ten monitoring points symmetrically at the upstream face and downstream face of the wall, shown in Figure 1(b)

Table 1 provides details of the monitoring instruments installed in the foundation and cutoff wall. The field instruments installed in the foundation included electromagnetic settlement gauges, displacement transducers and piezometers. The instruments installed in the wall included fixed inclinometers, strain meters and earth pressure cells. Figure 1(b) shows the instrument locations. Further details on the deployment of the monitoring system in the dam embankment and analyses of the monitored results are provided by Wen *et al.* (2017).

3. Analysis of monitoring results

3.1 Horizontal displacement and crest settlement measurements

Figure 4(a) shows the evolution of the horizontal displacement over time at the top monitoring points IN1-1, IN2-1 and IN3-1 (shown in Figure 1(b)). For comparison, the measured maximum horizontal displacements of several other cases are also plotted in the figure. To align the construction stages of different dams and for improved data comparability, the time at the start of reservoir filling for each case was set as the reference time. In Figure 4(a), the horizontal displacement of the wall of Miaojiaba dam was in the upstream direction. The displacement increased with time prior to reservoir filling, but the deformation rate gradually decreased. During dam construction, approximately 70% of the total displacement occurred in the first 3 months on average. The displacement gradually shifted towards the downstream direction under the effect of the water head pressure. Over 90% of the total downstream displacements ensued during the reservoir-filling stage, thereby indicating that water load significantly affected the deformation. Figure 4(b) shows the measured wall settlement along the wall crest axis of Miaojiaba dam and other dams at the end of the reservoir filling (EoF) stage. The wall settlement for Miaojiaba dam was small. The settlement was larger in the middle than near the abutments, with a maximum value of 2·0 cm at the middle of the wall top.

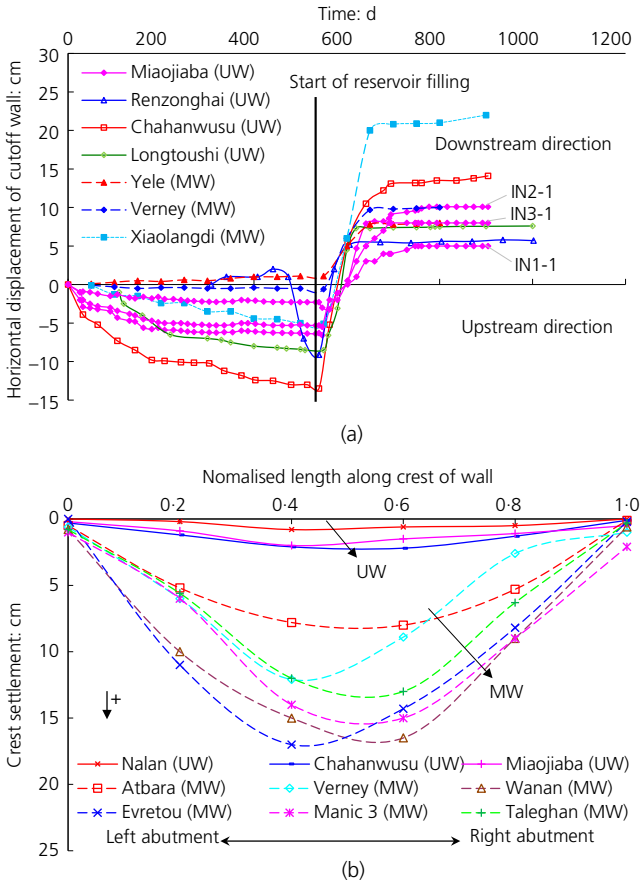

Figure 4. (a) Evolution of horizontal displacement over time at monitoring points IN1-1, IN2-1 and IN3-1 and maximum horizontal displacements of several other dam cases. (b) Settlement along the wall crest axis for Miaojiaba dam and other cases at the EoF stage. Other cases: Yele dam, Xiaolangdi dam, Atbara dam, Wanan dam and Longtoushi dam (Wang *et al.*, 2008); Verney dam and Evretou dam (Rice and Duncan, 2010b); Chahanwusu dam (Wen *et al.*, 2015); Renzonghai dam and Nalan dam (Li *et al.*, 2007); Manic 3 dam (Dascal, 1979); Taleghan dam (Arnold *et al.*, 2011)

In Figure 4, MW (middle wall) refers to the cutoff wall located in the middle of the dam base for dams with corewalls or inclined corewalls; UW (upstream wall) refers to the cutoff wall located at the upstream face of the dam. As shown in the figure, the upstream cutoff walls for the other CFRDs showed a deformation pattern similar to that of Miaojiaba dam. The walls generated a large horizontal displacement at the end of dam construction (EoC) stage and at the EoF stage, but the settlement was relatively small. However, the cutoff walls for the dams with corewalls or inclined corewalls (middle walls) exhibited a

significantly smaller horizontal displacement at the EoC stage than those with upstream walls, and the settlement was significantly larger at the EoF stage. These differences can be explained by the various loading characteristics of the wall. For a middle wall, the horizontal displacement of the surrounding foundation soil is small, and the lateral earth pressure on the upstream and downstream surfaces of the wall is relatively small and symmetrical at the EoC stage. However, for an upstream wall, a large differential lateral earth pressure can be generated from the large horizontal displacement of the surrounding foundation soil. The differential water head pressure is responsible for the horizontal displacement of the wall after the reservoir filling. A middle wall is subjected to significant vertical earth pressure and downward shear friction under the action of the overlying embankment, whereas the vertical load on the upstream wall is small considering the absence of overlying fill. The deformation behaviour of a cutoff wall is thus directly related to its location.

3.2 Vertical stress measurements

Figure 5 shows the progression of the vertical stress observed at monitoring points SM1-5, SM 2-5 and SM3-3 and the progression of the maximum vertical stress observed in several other dams. For Miaojiaba dam, the upstream face of the cutoff wall was in a compressive stress state during dam construction. The vertical compressive stresses in the downstream face decreased with time. Some tensile stresses were observed at the bottom of monitoring lines SM1 and SM3 in the downstream face, with maximum values of 1·6 MPa and 1·0 MPa at monitoring points SM1-5 and SM3-3, respectively, at the EoC stage. The tensile stress was due to the positive moment induced by the restricted bending deformation and the dragging effect exerted by the differential longitudinal deformation between the wall and the foundation. The vertical compressive stress in the downstream face began to increase after the start of reservoir filling and tended to stabilise after reservoir filling. The bending downstream deformation caused tensile stress in the upstream face of the wall at the EoF stage. Tensile stress appeared mainly at the bottom and abutments, with maximum values of 1·2, 0·1 and 1·5 MPa at monitoring points SM1-5, SM2-5 and SM3-3, respectively.

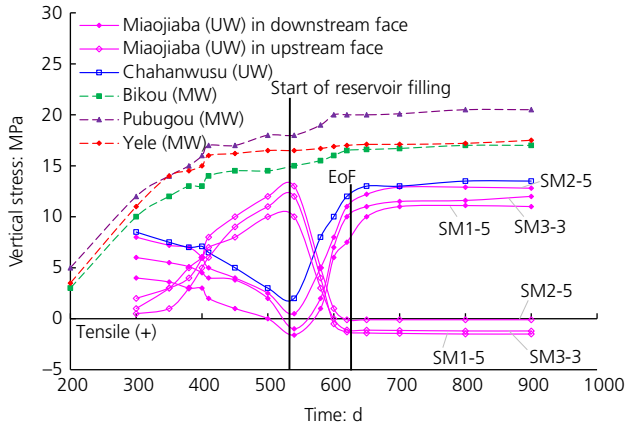

Figure 5. Progression of vertical stress observed at monitoring points SM2-1, SM 2-2 and SM2-3 in the downstream face of the cutoff wall and the progression of the maximum vertical stress observed in several other cases: Yele dam, Pubugou dam and Bikou dam (Wang *et al.*, 2008); Chahanwusu dam (Wen *et al.*, 2015)

The measured vertical stress of Chahanwusu dam exhibited a similar evolution progression to that of Miaojiaba dam, but the middle walls displayed a significantly different progression. The vertical stress in the downstream face accumulated over time. The progression and distribution of the vertical stress in the upstream face of the wall in some cases were similar to those of the downstream face. The middle cutoff walls were mainly in a compressive stress state. These stress distribution differences were due to the different loading characteristics of the wall in various positions.

4. Numerical model

4.1 Plastic-damage model for concrete cutoff walls

The observed results of the cutoff wall of Miaojiaba dam showed that large tensile stresses distributed in the wall may cause damage or cracking. A finite-element (FE) analysis was conducted to investigate the cutoff wall behaviour further. Concrete exhibits a linear elastic behaviour only under small load(s), and cracking and damage will occur with an increase in tensile strain (Xu *et al.*, 2015). Concrete damage should be considered when analysing the behaviour of high-strength concrete cutoff walls for high dams. The plastic-damage model proposed by Lee and Fenves (1998) was adopted to describe the behaviour of the concrete wall. This model can reveal the independent compressive and tensile damage patterns and stiffness restoration, and has been used in FE damage analyses on the face slabs of CFRDs (Dakoulas, 2012; Xu *et al.*, 2015). Only the main components of the model are introduced here; details can be found elsewhere (Lee and Fenves, 1998).

The stress–strain relationship is expressed as

$$1. \quad \sigma = (1-d)\bar{\sigma} = (1-d)E_{\mathrm{i}}(\varepsilon - \varepsilon^{\mathrm{p}})$$

where σ is the stress of the concrete, d is a scalar degradation damage variable that represents decreased elastic stiffness, $\bar{\sigma}$ is the effective stress, E_{i} is the undamaged elastic stiffness, ε id the total strain and ε^{p} is the plastic strain.

The damage variable (k_{n}) is introduced to describe the damage states. The degradation damage variable can be expressed as

$$2. \quad k_{\mathrm{n}} = \frac{1}{g_{\mathrm{n}}}\int_0^{\varepsilon^{\mathrm{p}}} \sigma_{\mathrm{n}} \mathrm{d}\varepsilon^{\mathrm{p}}; \quad g_{\mathrm{n}} = \int_0^{\infty} \sigma_{\mathrm{n}} \mathrm{d}\varepsilon^{\mathrm{p}}$$

$$3. \quad d = 1 - (1 - d_{\mathrm{C}}k_{\mathrm{C}})(1 - sd_{\mathrm{T}}k_{\mathrm{T}})$$

in which n represents the state (n = T indicates the tension state and n = C represents the compressive state), g_n is the dissipated energy density of the concrete (g_n can also be derived from the ratio of the fracture energy (G_n) to the characteristic length (l_n) determined from the size of an individual mesh element), σ_n is uniaxial stress, d_T and d_C are the tension and compressive uniaxial damage variables, k_T and k_C are the tension and compressive damage variables and s is a weight factor.

The results from other tensile and compressive loading experiments were simulated to validate the performance of the model. As shown in Figure 6, the numerical results were found to be consistent with the experimental data (Gopalaratnam and Shah, 1985; Karsan and Jirsa, 1969; Kupfer *et al.*, 1969) and the plastic-damage model was thus verified as being capable of describing the stress–strain behaviour of the concrete. In this work, the tensile strength and fracture energy were set to 2·01 MPa and 325 N/m, respectively, following previous studies that addressed similar concrete materials (Xu *et al.*, 2015; Yu *et al.*, 2015). The characteristic length (l_n) was determined to be 0·24 m based on the size of the mesh elements of the cutoff wall. The results obtained indicated large tensile stress, but the compressive stress was relatively small. Thus, only tensile damage of the wall was considered. The face slab, plinth and connection plate were considered to be linearly elastic. The density, elastic modulus, Poisson's ratio and hydraulic conductivity were 2·45 g/cm^3, 28 GPa, 0·167 and $1·0 \times 10^{-12}$ m/s, respectively.

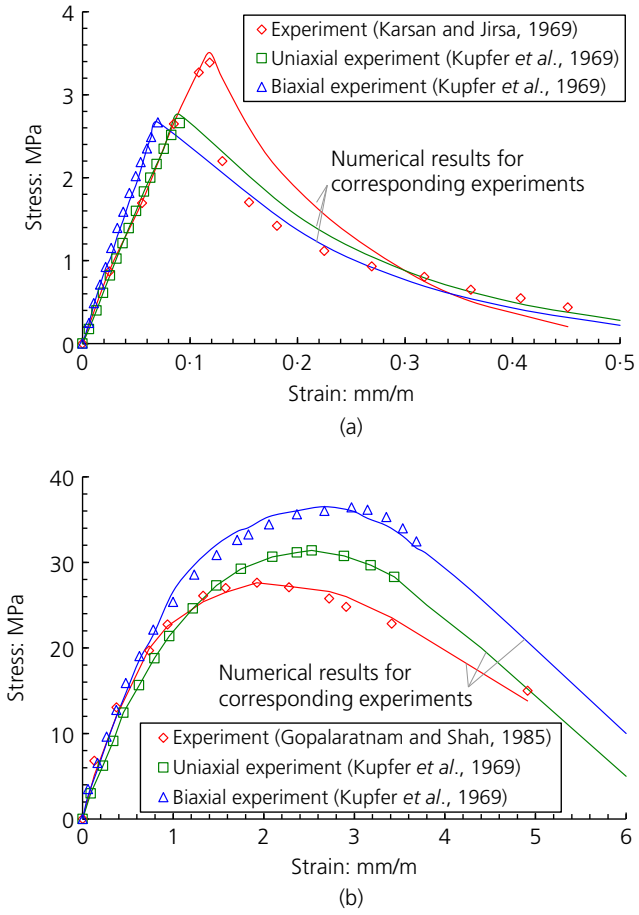

Figure 6. Uniaxial and biaxial loading: comparison of (a) tensile test simulation and (b) compressive test simulation with experimental results

For comparison, a linear elastic analysis of an ordinary concrete (OC) wall was also performed (density 2·45 g/cm^3, elastic modulus 26 GPa and Poisson's ratio 0·167). The elastic modulus was obtained through a uniaxial compression test. To compare the performance of the wall constructed with plastic concrete (PC), a linear elastic analysis of the PC wall was also performed. PC is more deformable than OC due to the addition of bentonite. The elastic modulus of PC is generally between 0·5 and 2·5 (Hinchberger *et al.*, 2010; Li *et al.*, 2007). The density, elastic modulus and Poisson's ratio of the PC were set to 2·20 g/cm^3, 1·5 GPa and 0·25, respectively, in accordance with previous research (Yu *et al.*, 2015). The initial hydraulic conductivity of the wall was set to $1·0 \times 10^{-9}$ m/s.

4.2 Elastoplasticity model for rockfill and alluvium

Triaxial experiments conducted on rockfill and alluvium specimens revealed that (*a*) the compressibility decreased with an increase in normal stress, (*b*) the deviatoric stress and axial strain curve increased with confining pressure and (*c*) the volumetric strain changed from dilation to contraction with an increase in confining pressure. A two-yield-surface elastoplasticity model (Zhang *et al.*, 2007) was used to describe the volumetric strain behaviour. Two yield surfaces were adopted to judge whether plastic strain occurred.

The model parameters obtained from the triaxial test results are listed in Table 2. For further details, the reader is referred to the work of Wen *et al.* (2017) for a comparison of model predictions and triaxial test results for the alluvium material.

4.3 Interface model

The interactions between the face slab and the dam embankment, the plinth and the foundation and the cutoff wall and the alluvium soil were modelled using the no-thickness friction contact method (Bathe, 2003) based on contact mechanics. The augmented Lagrange multiplier method was adopted for the frictional contact problems. Sliding between the structure and the soil was unrestricted by the grid because of discontinuity. Thus, this method could capture the contact and discontinuity behaviour of the soil–structure interface. The normal contact pressure (P) can be calculated from

$$P = \begin{cases} 0, & \mu_n > 0 \\ K_n \mu_n + \lambda_{i+1}, & \mu_n \leq 0 \end{cases} \quad (4)$$

Table 2. Parameters of the elastoplasticity model and the initial hydraulic conductivity

Material	Density: g/cm^3	K	m	ϕ_0: degrees	$\Delta\phi$: degrees	R_f	G_0	F_0	D_0	k_0: m/s
Cushion	2·25	1400	0·42	48	8·6	0·86	0·43	0·30	5·5	$1·5 \times 10^{-6}$
Transition	2·23	1300	0·42	49	8·7	0·87	0·41	0·28	5·2	$2·1 \times 10^{-4}$
Main rockfill	2·35	1250	0·45	53	8·5	0·89	0·37	0·25	5·2	$3·2 \times 10^{-3}$
Sub rockfill	2·25	1050	0·35	51	8·4	0·80	0·35	0·26	5·0	$1·9 \times 10^{-3}$
Q_4^{a1}	2·20	1000	0·43	43	8·6	0·78	0·30	0·23	4·6	$1·7 \times 10^{-4}$
Q_4^{a2}	2·15	1200	0·43	42	8·6	0·80	0·38	0·26	5·1	$1·7 \times 10^{-4}$
Q_4^{a3}	2·20	1500	0·42	42	8·5	0·81	0·42	0·33	5·3	$1·4 \times 10^{-4}$

5. $$\lambda_{i+1} = \begin{cases} \lambda_i + K_n \mu_n, & |\mu_n| \le \varepsilon_0 \\ \lambda_i, & |\mu_n| > \varepsilon_0 \end{cases}$$

where ε_0 is the invasion tolerance, λ_i is the Lagrange multiplier of iteration step i, K_n is the normal contact stiffness and μ_n is the distance between two contact faces.

The friction contact method was used to simulate direct shear tests on the interface behaviour between the face slab and the cushion layer in Zipingpu dam (Zhang and Zhang, 2009) and Shuibuya dam (Chen *et al.*, 2011). The results (Figure 7) showed that the agreement was quite reasonable except for a few data points, thus indicating that the friction contact method can capture the primary soil–structure interface behaviour. Given insufficient test results, certain parameters used in the present work were determined on the basis of previous studies and experience. When performing numerical calculations, the friction coefficient between a cutoff wall and alluvium soil is recommended to be 0·2 (Li *et al.*, 2007). Thus, in the interface model, the frictional coefficient was set to 0·2 and the contact tolerance was set to 0·5 mm.

To reconcile the difference in the settlement between the top of the cutoff wall and the plinth, a connection plate was constructed as a connecting structure between the cutoff wall and the plinth in Miaojiaba CFRD (Figure 8). The top of the wall

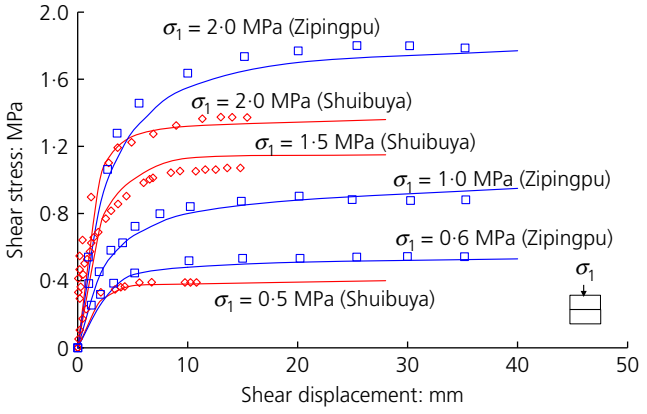

Figure 7. Comparison of the model predictions (curves) of the shear relationship with test results (open symbols)

was flush with the connecting plate. Joints were constructed where the connection plate met the plinth and the top of the cutoff wall to allow for their relative movement. The deformation modes of the joints included opening displacement and relative sliding (including shear deformation along the joint direction and differential settlement perpendicular to the joint). The friction contact method was also used to simulate the contact behaviour of the joints between the connection plate and the cutoff wall or plinth.

4.4 Coupled HM method

The alluvium foundation of Miaojiaba dam is typically a coarse granular material with high permeability. The HM coupling process could significantly affect the cutoff wall behaviour. To consider the HM coupling effect, the coupled HM analysis method proposed by Chen *et al.* (2011) was adopted in the present work. The coupled seepage and stress process was governed by the momentum and mass conservation laws of continuum mechanics, with the governing equations

6. $$\begin{cases} \nabla \cdot \left[\boldsymbol{D} : \nabla \left(\dfrac{\partial \boldsymbol{u}}{\partial t} \right) - \alpha \dfrac{\partial p_w}{\partial t} \boldsymbol{\delta} \right] + \dfrac{\partial \boldsymbol{f}_b}{\partial t} = 0 \\ [1 - H(\phi - z)] \rho_w \left(\dfrac{\partial \varepsilon_v}{\partial t} + S_w \dfrac{\partial \phi}{\partial t} \right) + \nabla \cdot (\rho_w \boldsymbol{v}) = 0 \end{cases}$$

In which ϕ is the total water head, $\boldsymbol{v}$ is the flow velocity, ρ_w is the water density, S_w is the specific storage, $\boldsymbol{u}$ is the displacement vector, p_w is the pore water pressure, $\boldsymbol{D}$ is the tangential elastic modulus tensor, α is Biot's coefficient, $\boldsymbol{f}_b$ is the body force tensor, $H(\phi\text{-}z)$ is a Heaviside function, ε_v is the volume strain, $\boldsymbol{\delta}$ is the Kronecker delta tensor, and t is the time.

The permeability variation to deformation was characterised by a modified Kozeny–Carman equation, where the evolution of porosity was linked to the volume strain.

7. $$\begin{cases} k = k_0 \left(\dfrac{n_i}{n_0} \right) \left(\dfrac{1 - n_0}{1 - n_i} \right)^2 \\ n_i = 1 - (1 - n_0) \exp(\beta_1 \varepsilon_v) \end{cases}$$

Here, n_i is the current porosity, n_0 is the initial porosity, k is the current hydraulic conductivity, k_0 is the initial hydraulic

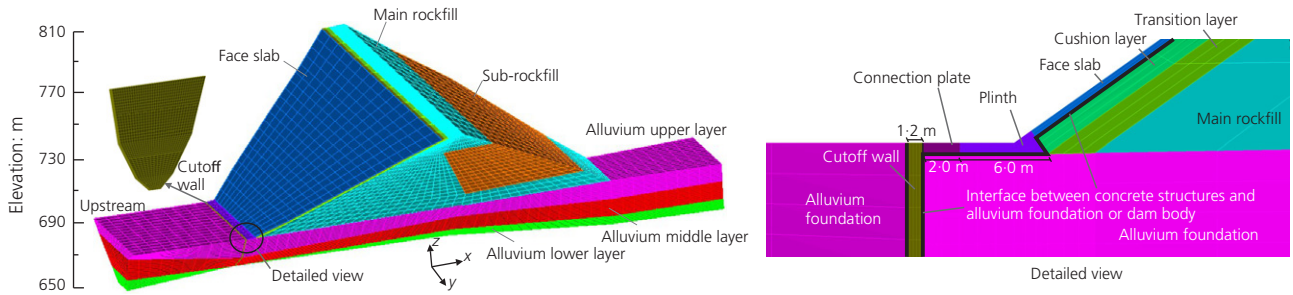

Figure 8. 3D FE mesh of the model

conductivity and β_1 is a coefficient ($\beta_1 = 1$ if the grains are assumed to be non-deformable). The initial hydraulic conductivities obtained through field tests are listed in Table 2.

An HM coupling process for analysing the deformation and seepage behaviour of a CFRD was developed using the described models. An interlaced algorithm was adopted to solve the coupled non-steady seepage flow and stress–strain processes sequentially. Details of the iteration method are provided by Chen *et al.* (2011). In each time step, the seepage flow process was initially solved through the variational inequality approach and then the mid-point incremental method was used to solve the non-linear mechanical process. The permeability was updated after the mechanical process at each time step. The iterations were terminated when the convergence criteria were satisfied for both processes at each time step.

4.5 FE model

A 3D FE mesh was constructed, as illustrated in Figure 8. The mesh contained 44 870 elements and 49 936 nodes; 6425 elements were used to model the cutoff wall. Five rows of elements were divided in the thickness direction to capture the behaviour of the cutoff wall accurately. Spatial eight-node isoparametric elements were used to simulate the different materials. The dam embankment zone and the geological features were demonstrated in the model. The foundation was divided into three layers to consider the geological characteristics.

The step-by-step construction and the subsequent reservoir filling were simulated in the numerical model, as depicted in Figure 1(a). The time-step length was set in accordance with the construction schedule during dam construction: the construction progress was modelled with 26 steps of rockfill placement in layers and three steps of face slab installation. Each layer thickness was less than 5 m for rockfill placement. Afterwards, the time-step length was set to 10 d in accordance with the rising rate of the reservoir level. The bottom and side boundaries were constrained in the normal direction and as impermeable boundaries. The water head was prescribed on the basis of the reservoir level fluctuation on the surfaces submerged in water. Potential seepage boundaries satisfying Signorini's complementary condition were set as the remaining boundaries. Notably, unless otherwise stated, the results of the OC cutoff wall discussed in Section 5 refer to the findings of the plastic-damage analysis.

The cutoff wall in Miaojiaba dam was constructed using the panel-by-panel technique. Inherent vertical construction joints were placed between every two successive panels. Observations and experience from constructing cutoff walls showed that a small thickness of bentonite infill from the bentonite slurry typically adheres strongly to the side walls of the primary panels, which cannot be removed completely (Soroush and Soroush, 2005). Li *et al.* (2007) concluded that vertical construction joints do not remarkably influence the deformation of a cutoff wall but can slightly reduce the tensile stress, especially near the abutments. Brown and Bruggemann (2002) reported that cracks may occur through the bentonite infill given the differential movement between the panels and hydraulic fracture. In the present work, the effects of the vertical construction joints were disregarded in the numerical model considering the relatively wide valley and insufficient test data. Neglecting the vertical construction joints was a significant simplification in the numerical model. The adverse effects of vertical construction joints and bentonite infill on the mechanical behaviour of a wall might be expected and important in narrow valleys.

5. Results and discussion

5.1 Loads acting on the wall

The behaviour of a cutoff wall is mainly determined by the horizontal and vertical loads acting on the wall. The placement and compaction of the dam embankment change the stresses of the soil, thereby causing horizontal displacement of the foundation. Generally, significant lateral earth pressure differences between the upstream and downstream faces of a wall are induced by the large horizontal displacement of the surrounding foundation soil. Given that the compressibility is considerably lower in the walls than in the adjacent soil, a large settlement difference can be generated between them due to the top pressure, which causes significant shear friction at the interfaces. Observed results have shown that, under vertical earth pressure, the vertical stress is larger in the middle of a

cutoff wall than in the top (Brown and Bruggemann, 2002). The pressures measured in soil adjacent to the wall are lower than the overburden pressure (O'Neal and Hagerty, 2011). Dascal (1979) concluded that 85% of the vertical stresses in the middle wall is induced by shear friction. These results indicate that shear friction affects wall behaviour significantly. Shear friction is mainly determined by the relative settlement and lateral earth pressure.

Figure 9 shows the depth distributions of the settlement of the wall and adjacent soil, lateral earth pressure and shear friction acting on the deepest cross-section of the wall. During dam construction, the soil near the downstream face of the wall was compressed but that near the upstream face was uplifted, with a simulated maximum upward displacement of 5·0 cm at the top. The main reason for this outcome is that upstream soil will withstand horizontal thrust from the wall. At the EoC stage, the simulated maximum settlement of the soil at the top of the downstream face was 6 cm, which was larger than the simulated wall settlement of 1·5 cm. Upon subsequent reservoir filling, both soils were compressed under the effect of the water load. The ratios of the relative settlement at the top of the upstream and downstream faces were determined to be 3·7 and 2·4, respectively.

The distribution of the lateral earth pressure along the wall was non-linear with depth. Given the larger horizontal displacement of the adjacent soil, the earth pressure was large at the centre. The simulated maximum pressure at the EoC stage was 0·73 MPa, which was smaller at the upstream face than at the downstream face (0·98 MPa). The upstream and downstream faces showed decreased pressures at the EoF stage in comparison with those at the EoC stage. These changes were related to the pore water pressure acting on the wall. The simulated pressures were near the measured values at the EoC and EoF stages, thereby indicating that the friction contact method can capture the primary soil–structure interface behaviour.

The wall experienced upward shear friction at the upstream face and mainly downward shear friction at the downstream face, due to the relative deformation between the wall and the adjacent soil at the EoC stage, as exhibited in Figure 9. The simulated maximum downward shear friction at the downstream face was 0·47 MPa, which was larger than the upward shear friction at the upstream face. Reservoir filling changed the shear friction pattern. The wall mainly experienced downward shear friction with a simulated maximum value of 0·1 MPa at the top of the upstream face and 0·4 MPa at the top of the downstream face. The wall movement comprised compression deformation and rigid body movement, but the compressive deformation at the bottom of the alluvium was constrained by the bedrock. Therefore, the movement at the bottom may be larger for the wall than for the adjacent soil. The downward shear friction was reduced to zero at the depth where the wall and the alluvium equally settled. This depth is called the neutral point. Below this depth, upward shear friction was generated. The position of the neutral point was near the bottom, approximately 1·5 m above the bedrock, which moved upwards by approximately 1·5 m at the EoF stage.

As shown in Figure 9, the simulated settlement was considerably larger in the PC wall than in the OC wall. The maximum relative settlement ratio did not exceed 1·5, thereby resulting in a significant reduction of the shear friction. Given that the elastic modulus of the PC was small, the wall and soil together bore the vertical loads. The lateral earth pressures for the PC wall at the EoC stage were larger than for the OC wall in the upstream face but were smaller in the downstream face. The results were the opposite at the EoF stage. The horizontal displacement of the OC and PC walls was similar, but their stiffness characteristics were different, thus causing the difference in lateral earth pressures.

5.2 Deformation behaviour of the concrete cutoff wall

Figure 10 shows the horizontal deformation shape and displacement along the three monitoring lines at the EoC and EoF stages. The figure shows that the top of the wall bent a maximum of 7·0 cm in the upstream direction at the EoC stage and a maximum of 10·0 cm in the downstream direction at the EoF stage. The horizontal displacement at the bottom was small considering the restrictive effect of the surrounding bedrock. This deformation trend would cause positive moments at the abutments and the bottom of the wall in the downstream face at the EoC stage and in the upstream face at the EoF stage. The simulated deformation trends and values at the monitoring lines were consistent with the field measurements, thereby indicating that the numerical model could be used to analyse the deformation behaviour of the wall.

As shown in Figure 10, the horizontal displacements for the PC wall were similar to those for the OC wall, showing quite large deformations because the wall's horizontal displacement was directly determined by the horizontal displacement of the adjacent soil. The simulated results were compared with the results without considering the HM coupling effect, where the water pressure was simulated as surface forces and applied to the impervious system. At the EoF stage, the simulated horizontal displacements considering the HM coupling effect were larger than those without, with a maximum difference of approximately 3·0 cm. This indicates that the HM coupling effect has a certain effect on wall deformation. The effect of the HM coupling process is a result of two mechanisms. Firstly, the HM coupling effect affected the deformation of the alluvium foundation, thereby causing a change in the lateral earth pressure and shear friction of the wall, as exhibited in Figure 9(b). Secondly, the HM coupling analysis method could rigorously model the seepage effect on the cutoff wall behaviour.

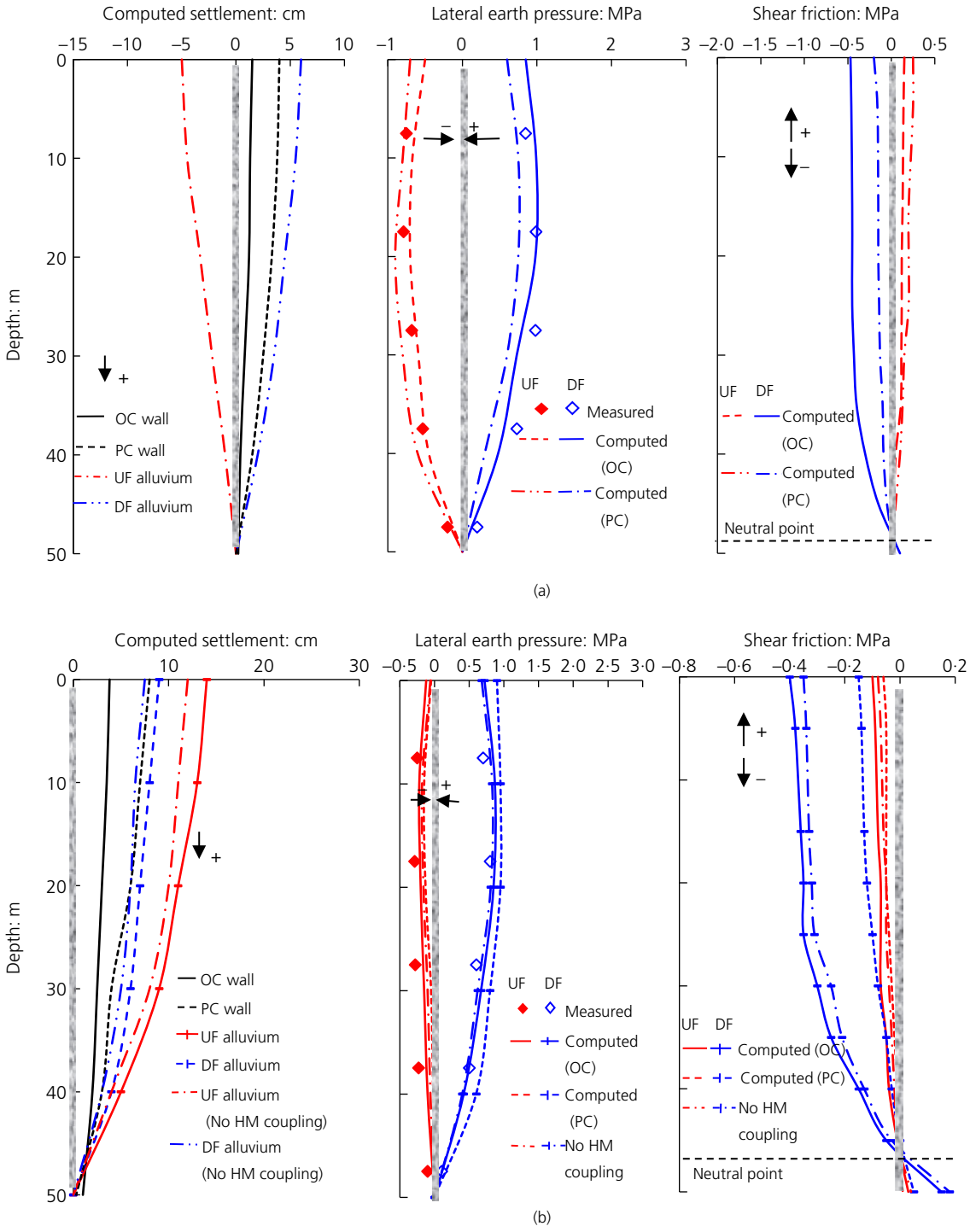

Figure 9. Depth distributions of the wall and adjacent soil settlement, lateral earth pressure and shear friction acting on the wall at the EoC stage (a) and EoF stage (b) (UF, upstream face of wall; DF, downstream face of wall)

5.3 Stress analysis of the concrete cutoff wall

Figure 11 shows the measured and simulated vertical stress distributions along the three monitoring lines in the upstream and downstream faces. The distributions of the major and minor principal stresses in the wall are shown in Figure 12. The abutments and the bottom of the downstream face of the wall presented tensile zones at the EoC stage. The cutoff walls exhibited simulated maximum compressive and tensile stresses of 20 MPa and 1·9 MPa, respectively, at the bottom of the wall near the abutments. These values did not exceed the

material strength. The downstream face gradually transitioned into a compressive stress state during reservoir filling. At the EoF stage, tensile zones developed at the abutments of the upstream face. The simulated maximum compressive and tensile stresses were 22 MPa and 2·0 MPa, respectively. The tensile stress at the different stages was mainly caused by the positive moment induced by the restricted bending deformation and the dragging effect exerted by the differential longitudinal deformation between the wall and the foundation. The values of vertical compressive stress increased from the top to the bottom of the wall at the section near the abutments. At the deepest cross-section, the vertical compressive stress increased to the neutral point position due to the downward shear friction, and the stress gradually decreased towards the bottom of the wall because of the development of upward shear friction. These results show that the most dangerous section is not located in the middle of the river bed but at the abutments. The walls mainly bore the bending effect under the load of the water head and lateral earth pressures, and experienced significant tensile stress during both dam construction and reservoir filling. These stress distributions were significantly different from those for the middle wall. Dascal (1979) and Yu *et al.* (2015) reported that middle walls are mainly exposed to the compressive stress state and tensile stress only appears at the tip of the upper part of the wall due to restricted deformation.

The measured vertical stresses in the upper part of the wall were close to the simulated values, whereas those in the lower part of the wall were lower than the simulated values. This irregularity is attributed to the limitations of the numerical model (e.g. the simplification of the geometric model, inadequate constitutive model and the difficulty in considering complex loading and ground conditions). The vertical stress was substantially smaller for the PC wall than for the OC wall, considering its low elastic modulus compared with that of the foundation. At the EoF stage, the maximum vertical compressive and tensile stresses in the downstream face decreased from

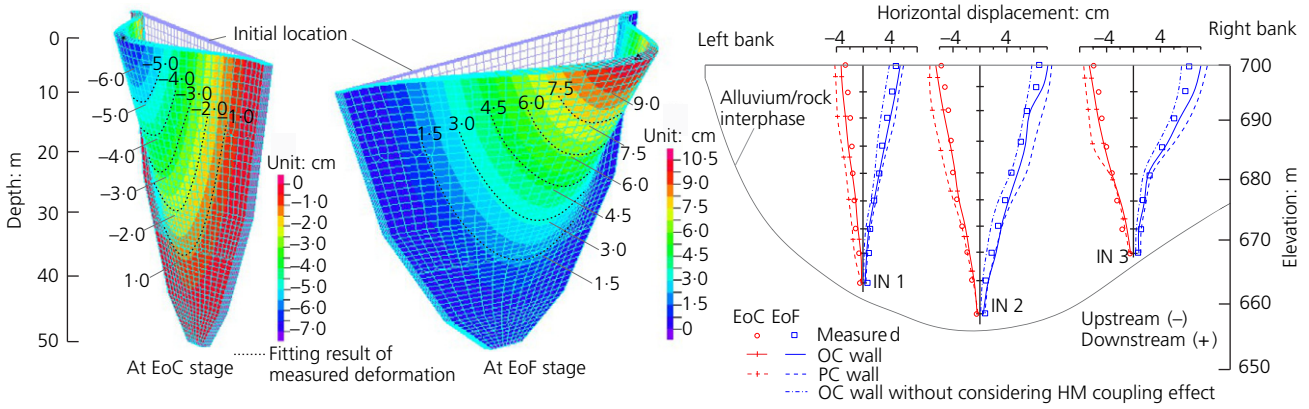

Figure 10. Horizontal deformation and simulated and measured horizontal displacements along the three monitoring lines

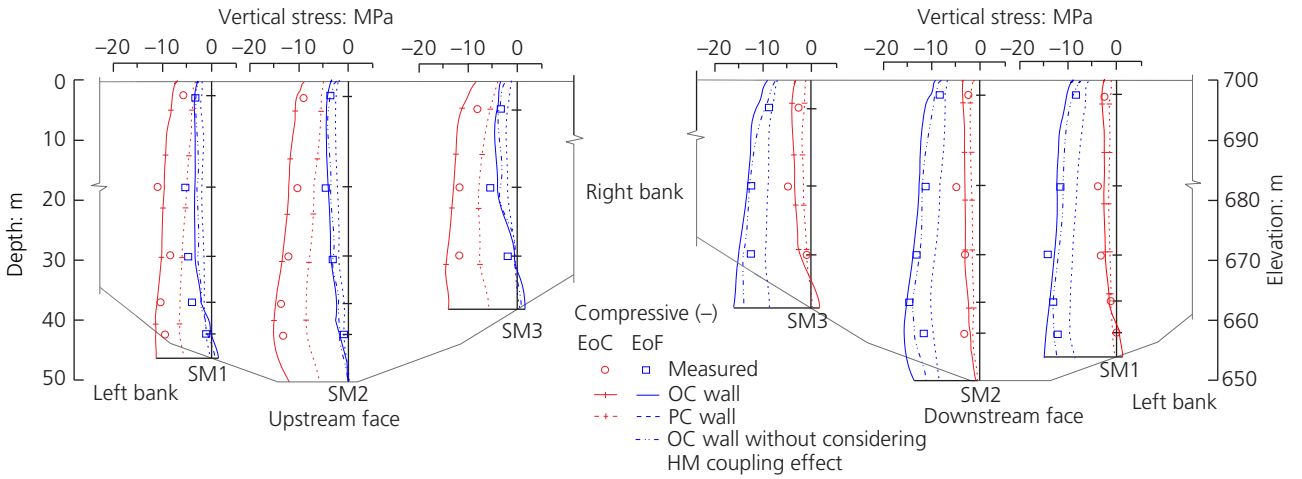

Figure 11. Vertical stress distribution along the three monitoring lines in the upstream and downstream faces

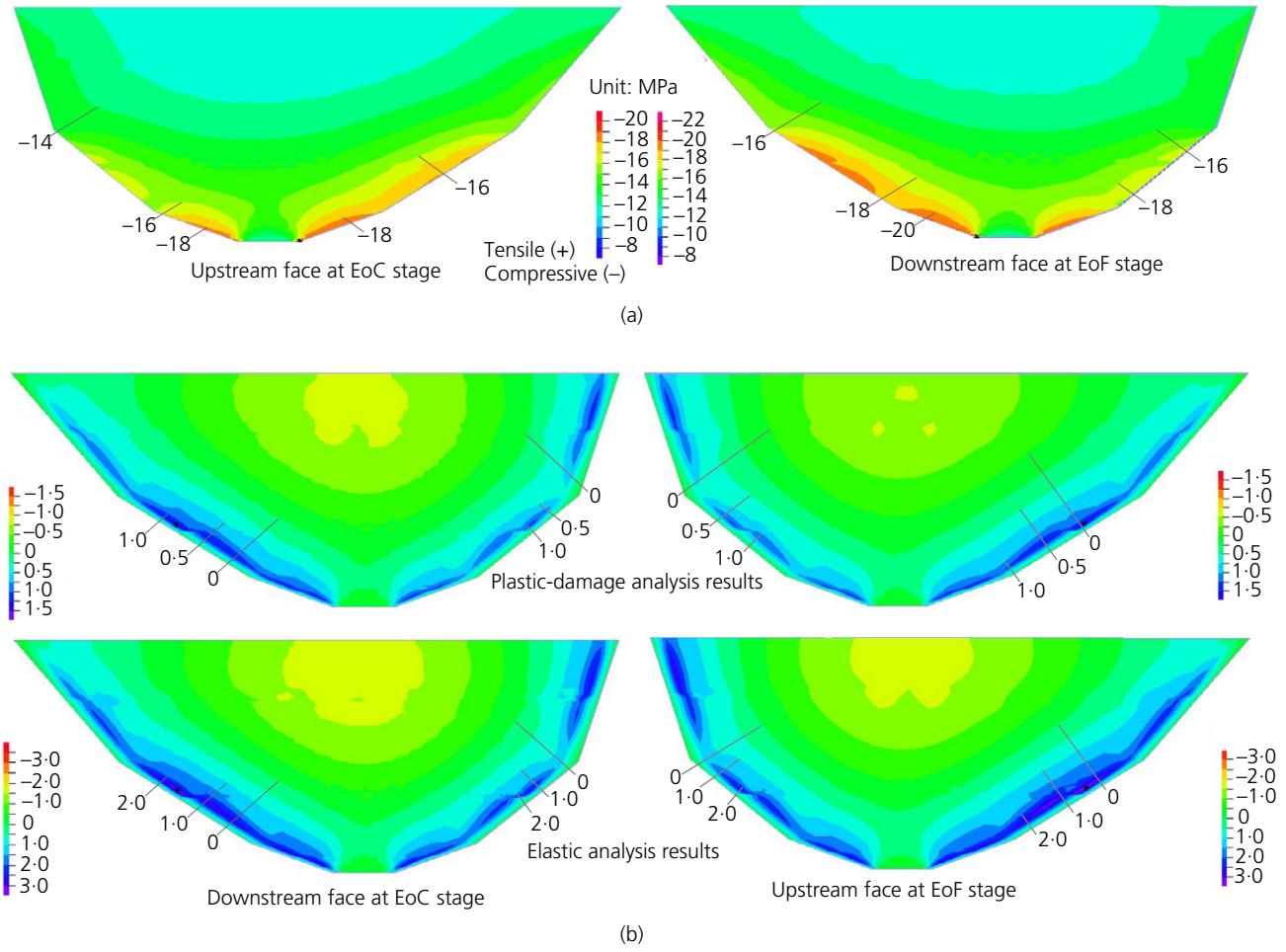

Figure 12. (a) Major principal stress distribution and (b) minor principal stress distribution at different stages

18 MPa to 10 MPa and from 1·8 MPa to 0·1 MPa, respectively. These results indicate that the use of PC material can significantly improve the stress state of the wall. In addition, the simulated vertical stresses considering the HM coupling effect were generally larger than those without. The maximum difference in the compressive stress in the downstream face and the tensile stress in the upstream face at the EoF stage was 4·0 MPa and 0·5 MPa, respectively, thus indicating that the HM coupling effect did influence the wall stress, but the difference was insignificant.

Figure 12(b) shows a comparison of the minor principal stress distribution from the plastic-damage and linear elastic analyses to estimate the influence of the concrete model on wall behaviour. A larger tensile stress was observed when using the elastic model rather than the plastic-damage model. The maximum tensile stress at the EoC and EoF stages was over 3.0 MPa, which exceeded the tensile strength. The linear elastic model uses Young's modulus and Poisson's ratio to describe the mechanical behaviour of the concrete cutoff wall. The linear elastic model cannot model cracking or damage, and both phenomena occur when the tensile or compressive stresses induced in the cutoff wall exceed its tensile or compressive strength. Therefore, the stress distributions obtained by the linear elastic model can be used to evaluate potential cracking risks in the cutoff wall. By contrast, the maximum tensile stresses of the wall obtained using the plastic-damage model rarely exceeded the tensile strength, and the tensile zone was significantly smaller. Stiffness degradation and stress redistribution occurred in the plastic-damage model when the tensile strength of the concrete was reached. Damage evolution and stress release and redistribution can be reasonably considered using the plastic-damage model. Therefore, in the concrete cutoff wall numerical simulations, the plastic-damage model offers an improvement on the elastic model.

5.4 Plastic-damage analysis and cracking of the concrete cutoff wall

A concrete cutoff wall will crack or fail when the compressive or tensile stresses induced in the wall exceed the capacity of the

material. The simulated maximum compressive stress was 73% of the compressive strength. According to the elastic analysis, none of the stresses exceeded the compressive strength, thereby indicating that compressive stress only slightly affected the safety of the cutoff wall in the Miaojiaba project. This section primarily focuses on tensile damage that may result in crack propagation.

Figure 13 illustrates the tensile damage distribution (denoted by the damage variable k_T) in the wall. During dam construction, tensile damage occurred at the bottom and near the abutments in the downstream face. After reservoir filling, tensile damage appeared at the bottom and near the abutments in the upstream face. In Figure 12(b), the maximum minor principal stress computed by the linear elastic and plastic-damage models appeared at the corresponding positions at the EoC and EoF stages. The results exhibited favourable agreement and thus corroborate each other. The tensile damage zone occurred intensively at the bottom and near the abutment, and large portions of the wall were not damaged or were only slightly damaged ($k_T < 0{\cdot}1$). The tensile damage observed was worse at the EoF stage than at the EoC stage. The maximum tensile damage rarely exceeded 0·8 in the elements, thus denoting that cracking will not occur (Lee and Fenves, 1998). The simulated damage distribution and the cracking potential were different from those of middle walls. Yu *et al*. (2015) analysed the tensile damage of a middle cutoff wall and found that tensile damage was mainly localised at the tip of the upper part during dam construction and propagated to bending locations on the downstream face near the bedrock after reservoir filling. Rice and Duncan (2010b) reported that the differential water pressure that acts across a seepage barrier is of sufficient magnitude to cause cracking in a middle wall, with the most likely location for cracking at the interface between the alluvium and the bedrock.

Table 3 lists the failure or cracking of cutoff walls of seven in-service dams. The failures in the wall of dams with corewalls were compressive failures, with such failure mainly observed at the bottom. For this wall type, the overlying earth pressure and shear friction from the adjacent alluvium are the main causes of excessive compressive stress. For the wall of dams with inclined walls or CFRD-type dams, failures were mainly tensile or shear cracks. Cracks occurred at the top or bottom where the wall comes into contact with the bedrock, with bending deformation being the main source of the cracks. These results are consistent with those of Brown and Bruggemann (2002) who reported that hydraulic fracture is more likely to occur in an upstream wall given the bending effect. As shown in Table 3, cracks were rarely observed in PC walls, due to its small elastic modulus that is comparable to the elastic modulus of an alluvium foundation (Rice and Duncan, 2010b; Yu *et al*., 2015).

6. Conclusions

This paper has described a study based on in situ measurements and numerical analysis of the behaviour of a concrete cutoff wall for a CFRD built on an alluvium foundation. The ability of a 3D numerical model to predict the cutoff wall behaviour and the effects of the concrete material and the HM

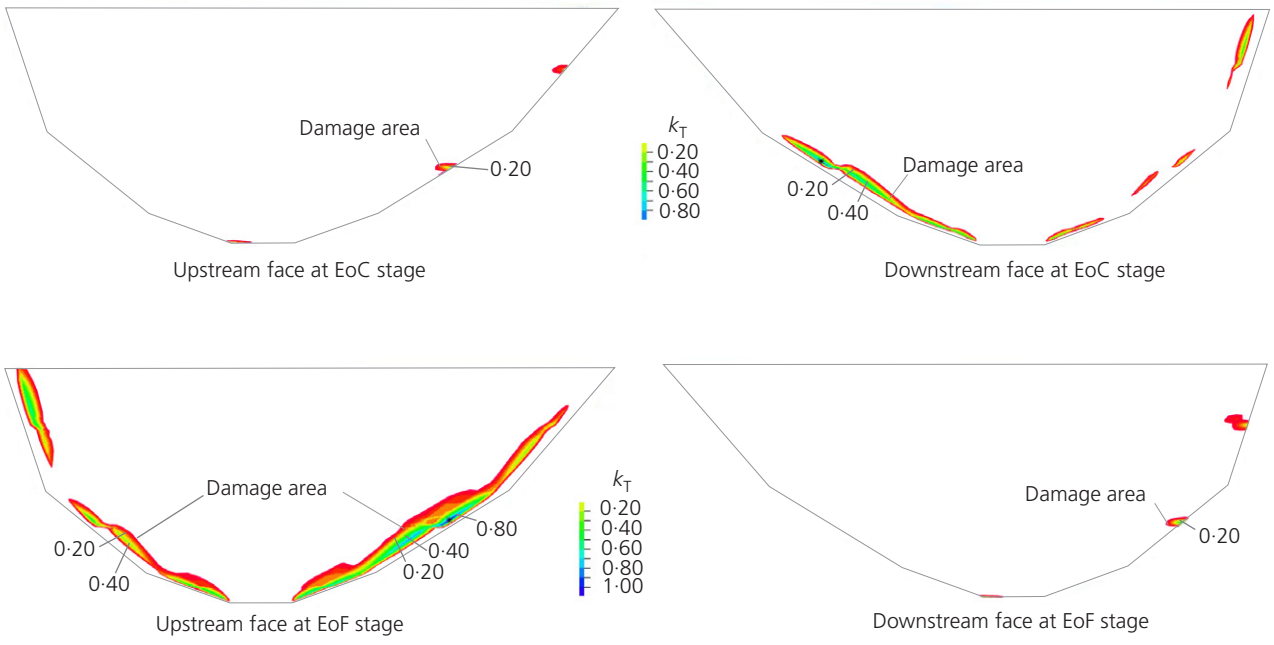

Figure 13. Tensile damage distribution (denoted by damage variable k_T) of the concrete cutoff wall at EoC and EoF stages

Table 3. Precedent concrete cutoff wall with failure or cracking

Project	Dam type[a] and year of construction	Depth and material	Issue	Cause	Reference
Arminou	DC, 1999	16 m, PC	Vertical joint cracks and erosion	Bentonite infill and internal erosion	Brown and Bruggemann (2002)
Cetian	DC, 1989	39 m, OC	Cracks at the bottom after EoF	Deformation and compressive stress	Li *et al.* (2007)
Kezier	DI, 1998	40 m, OC	Some cracks at top after EoF	Bending deformation in downstream direction	Rice and Duncan (2010b)
Manic 3	DC, 1976	131 m, OC	Extrusion damage near bedrock after EoF	Inconsistent deformation of the wall and foundation	Dascal (1979)
Niutoushan	CFRD, 1989	62·5 m, OC	Local damage and cracks at top	Bending deformation and tensile stress	Wang *et al.* (2008)
Ravi	DI, 1968	88 m, OC	Shear and tensile damage at bottom after EoF	Longitudinal deflection deformation	Wen *et al.* (2018)
Shawan	DC, 2000	64 m, OC	Infiltration damage at bottom during reservoir filling	Improper construction	Wang *et al.* (2008)

[a]DI, dam with inclined walls; DC, dam with corewalls

coupling effect on the wall behaviour were discussed. On the basis of the results obtained in this work, the following conclusions were drawn.

(*a*) The concrete cutoff wall in Miaojiaba CFRD bore a bending effect under the load of the water head and lateral earth pressures, and experienced significant tensile stresses at the bottom in the downstream face at the EoC stage and at the bottom and abutments in the upstream face at the EoF stage. The tensile damage zone occurred at the bottom and near the abutment of the wall, but no cracking developed in the wall. These results indicate that the wall deformation and stress are within a reasonable range and the wall will perform well.

(*b*) The behaviour of a cutoff wall for a CFRD was evaluated to be significantly different from that of a wall in the middle of the dam base. Middle walls are subjected to a compression effect and exposed to compressive stress, which may induce compressive failures at the bottom. However, for upstream walls, tensile or shear cracks can occur at the bottom or at the abutments. The location of the cutoff wall is thus a deterministic factor affecting the behaviour of the wall.

(*c*) The use of PC material could significantly improve the stress state of the wall. The HM coupling effect resulted in large deformation and tensile stress in the wall.

(*d*) The plastic-damage model was considered to provide a reasonable basis for damage evaluation of a concrete cutoff wall. The model can be used to evaluate damage in other concrete seepage control structures, including the face slab, plinth and junction plate. The simulated deformations and stresses at the monitoring points were consistent with the field measurements, thereby indicating that the numerical model provides a reasonable basis for damage evaluation of concrete cutoff walls.

Acknowledgement

This study was supported by the National Natural Science Foundation of China (Grant No. 51722907), Scientific Research Program Funded by Shaanxi Provincial Education Department (Program No. 19JS047) and National Natural Science Foundation of China (Grant Nos. 51579207 and 51879217).

REFERENCES

Abbaslou H, Ghanizadeh AR and Amlashi AT (2016) The compatibility of bentonite/sepiolite plastic concrete cut-off wall material. *Construction and Building Materials* **124**: 1165–1173.

Arnold M, Beckhaus K and Wiedenmann U (2011) Cut-off wall construction using cutter soil mixing: a case study. *Geotechnik* **34(1)**: 11–21.

Ata AA, Salem TN and Elkhawas NM (2015) Properties of soil–bentonite–cement bypass mixture for cutoff walls. *Construction and Building Materials* **93**: 950–956.

Bathe KJ (2003) *ADINA Theory and Modeling Guide*. ADINA R & D, Inc., Watertown, MA, USA.

Brown AJ and Bruggemann DA (2002) Arminou dam, Cyprus, and construction joints in diaphragm cut-off walls. *Géotechnique* **52(1)**: 3–13, https://doi.org/10.1680/geot.2002.52.1.3.

Bruce DA, Dreese TL, Harris MC and Heenan DM (2012) Composite cut-off walls for existing dams: theory and practice. In *Proceedings of the 4th International Conference on Grouting and Deep Mixing, New Orleans, LA, USA* (Johnsen LF, Bruce DA and Byle MJ (eds)). American Society of Civil Engineers, Reston, VA, USA, GSP 228, vol. 2, pp. 1248–1264.

Chegenizadeh A, Keramatikerman M, Santa GD and Nikraz H (2018) Influence of recycled tyre amendment on the mechanical behaviour of soil-bentonite cut-off walls. *Journal of Cleaner Production* **177**: 507–515.

Chen Y, Hu R, Lu W, Li D and Zhou C (2011) Modeling coupled processes of non-steady seepage flow and non-linear deformation for a concrete-faced rockfill dam. *Computers & Structures* **89(13)**: 1333–1351.

Dakoulas P (2012) Nonlinear seismic response of tall concrete-faced rockfill dams in narrow canyons. *Soil Dynamics and Earthquake Engineering* **34(1)**: 11–24.

Dascal O (1979) Structural behaviour of the Manicouagan 3 cutoff. *Canadian Geotechnical Journal* **16(1)**: 200–221.

Gopalaratnam VS and Shah SP (1985) Softening response of plain concrete in direct tension. *ACI Journal Proceedings* **82(3)**: 310–323.

Hinchberger S, Weck J and Newson T (2010) Mechanical and hydraulic characterization of plastic concrete for seepage cut-off walls. *Canadian Geotechnical Journal* **47(4)**: 461–471.

Karsan ID and Jirsa JO (1969) Behaviour of concrete under compressive loadings. *Journal of the Structural Division ASCE* **95(12)**: 2535–2563.

Kupfer H, Hilsdorf HK and Rusch H (1969) Behaviour of concrete under biaxial stresses. *ACI Journal Proceedings* **66(8)**: 656–666.

Lee J and Fenves GL (1998) A plastic-damage concrete model for earthquake analysis of dams. *Earthquake Engineering & Structural Dynamics* **27(9)**: 37–56.

Li NH, Mi ZK and Sun DW (2007) Study on affecting factors of stress-deformation of diaphragm walls for concrete face rockfill dams built on thick alluvium deposit. *Chinese Journal of Geotechnical Engineering* **29(1)**: 26–31.

Li YC, Cleall PJ, Wen YD, Chen YM and Pan Q (2015) Stresses in soil–bentonite slurry trench cut-off walls. *Géotechnique* **65(10)**: 843–850.

Moharrami A, Moradi G, Bonab MH, Katebi J and Moharrami G (2014) Performance of cutoff walls under hydraulic structures against uplift pressure and piping phenomenon. *Geotechnical and Geological Engineering* **33(1)**: 95–103.

O'Neal TS and Hagerty DJ (2011) Earth pressures in confined cohesionless backfill against tall rigid walls – a case history. *Canadian Geotechnical Journal* **48(8)**: 1188–1197.

Rice JD and Duncan JM (2010a) Deformation and cracking of seepage barriers in dams due to changes in the pore pressure regime. *Journal of Geotechnical and Geoenvironmental Engineering* **136(1)**: 16–25.

Rice JD and Duncan JM (2010b) Findings of case histories on the long-term performance of seepage barriers in dams. *Journal of Geotechnical and Geoenvironmental Engineering* **136(1)**: 2–15.

Rosen JB, Arnold MA, Bachus RC and Schauer PED (2011) GIS for geotechnical decision making: visualization of cut-off wall construction data. In *Proceedings of Geo-Frontiers 2011 Congress: Advances in Geotechnical Engineering, Dallas, TX, USA* (Han J and Alzamora PE (eds)). American Society of Civil Engineers, Reston, VA, USA, GSP 211, pp. 2907–2916.

Song H and Cui W (2015) Stop-end method for the panel connection of cut-off walls. *Proceedings of the Institution of Civil Engineers – Geotechnical Engineering* **168(5)**: 457–468.

Soroush A and Soroush M (2005) Parameters affecting the thickness of bentonite cake in cutoff wall construction: case study and physical modeling. *Canadian Geotechnical Journal* **42(2)**: 646–654.

Takai A, Inui T and Katsumi T (2016) Evaluating the hydraulic barrier performance of soil-bentonite cutoff walls using the piezocone penetration test. *Soils and Foundations* **56(2)**: 277–290.

Wang QY, Sun WG and Xiong H (2008) *Plastic Concrete Cutoff Walls.* China Water Conservancy and Hydropower Press, Beijing, China.

Wen L, Chai J, Wang X *et al.* (2015) Behaviour of concrete-face rockfill dam on sand and gravel foundation. *Proceedings of the Institution of Civil Engineers – Geotechnical Engineering* **168(5)**: 439–456.

Wen L, Chai J, Xu Z, Qin Y and Li Y (2017) Monitoring and numerical analysis of behaviour of Miaojiaba concrete-face rockfill dam built on river gravel foundation in China. *Computers and Geotechnics* **85**: 230–248.

Wen L, Chai J, Xu Z, Qin Y and Li Y (2018) A statistical analysis on the concrete cutoff wall behaviour. *Proceedings of the Institution of Civil Engineers – Geotechnical Engineering* **171(2)**: 160–173.

Xiao M, Ledezma M and Wang J (2016) Reduced-scale shake table testing of seismic behaviors of slurry cutoff walls. *Journal of Performance of Constructed Facilities* **30(2)**: 04015057.

Xu B, Zou D and Liu H (2012) Three-dimensional simulation of the construction process of the Zipingpu concrete face rockfill dam based on a generalized plasticity model. *Computers and Geotechnics* **43**: 143–154.

Xu B, Zou D, Kong X, Hu Z and Zhou Y (2015) Dynamic damage evaluation on the slabs of the concrete faced rockfill dam with the plastic-damage model. *Computers and Geotechnics* **65**: 258–265.

Yu X, Kong X, Zou D, Zhou Y and Hu Z (2015) Linear elastic and plastic-damage analyses of a concrete cut-off wall constructed in deep overburden. *Computers and Geotechnics* **69**: 462–473.

Zhang G and Zhang JM (2009) Numerical modeling of soil–structure interface of a concrete-faced rockfill dam. *Computers and Geotechnics* **36(5)**: 762–772.

Zhang G, Zhang JM and Yu Y (2007) Modeling of gravelly soil with multiple lithologic components and its application. *Soils and Foundations* **47(4)**: 799–810.

How can you contribute?

To discuss this paper, please email up to 500 words to the editor at journals@ice.org.uk. Your contribution will be forwarded to the author(s) for a reply and, if considered appropriate by the editorial board, it will be published as discussion in a future issue of the journal.

Proceedings journals rely entirely on contributions from the civil engineering profession (and allied disciplines). Information about how to submit your paper online is available at www.icevirtuallibrary.com/page/authors, where you will also find detailed author guidelines.